Chipless RFID Tag Using Hybrid Coding Technique

Arnaud Vena, Etienne Perret, *Member, IEEE*, and Smail Tedjini, *Senior Member, IEEE*

***Abstract*—Increasing the coding capacity of chipless RFID tags is a key factor while considering the development of miniaturized tags. A novel hybrid coding technique by combining phase deviation and frequency position encoding is proposed here. A coding capacity of 22.9 bits is obtained simply with five resonators within a reduced dimension of 2 cm × 4 cm. The proposed tag is based on 5 'C' like metallic strip resonators having resonance frequency within the band of 2.5 GHz to 7.5 GHz. The tag is potentially low-cost since only one conductive layer is needed for the fabrication. Different tag configurations are designed and validated with measurement results in bi-static configuration. A good agreement between measurement and simulation validates the theoretical predictions.**

***Index Terms*—"C" resonator, chipless RFID, frequency encoding, hybrid encoding, phase encoding, RFID.**

I. Introduction

RFID is a technology firstly introduced during the 2nd World War to identify friend and foe (IFF) aircrafts. The basic principle consists in identifying objects by means of reflected electromagnetic waves. Nowadays, the term RFID is largely used to denote numerous applications. Among them, pallet identification, road toll system, item tracking and fare collection system for travelers in urban transportation network are widely used. To fit these applications having various constraints in terms of environment, read range and defined standards, several tag technologies can be found in [1]. In the case of fare collection, passive tags are detected by magnetic near field coupling at 13.56 MHz, leading to a read range within 5 cm to 40 cm. In the case of pallet identification, the needed range is higher and can reach 10 m, thus, farfield passive tags are very desirable. Operating frequencies used are mainly in the UHF band around 900 MHz and 2.4 GHz but also in SHF band at 5.8 GHz [1]. For all these technologies, a transmission protocol is used between the reader and the tag. Data bits are sequentially exchanged in a half duplex format and the reader maintains the field to power the tag during both transmission and reception.

Manuscript received July 05, 2011; revised September 22, 2011; accepted September 26, 2011. Date of publication November 02, 2011; date of current version December 14, 2011. This work was supported by the French National Research Agency via the ANR-09-VERS-013 program. This paper is an expanded paper from the IEEE International Microwave Symposium, Baltimore, MD, June 5–10, 2011.

The authors are with the Laboratoire de Conception et d'Intégration des Systèmes (LCIS)/Grenoble Institute of Technology, Valence, France (e-mail: arnaud.vena@esisar.grenoble-inp.fr; etienne.perret@esisar.grenoble-inp.fr; smail.tedjini@esisar.grenoble-inp.fr).

Color versions of one or more of the figures in this paper are available online at http://ieeexplore.ieee.org.

Digital Object Identifier 10.1109/TMTT.2011.2171001

Item tracking and identification is one of the major challenges of UHF RFID because this market represents 10 trillions of units sold each year [2].

Competing with the optical barcode technology is a hard task for classical RFID tag having an antenna and a chip, whereas chipless RFID tag has a key role to reach this goal. Indeed, this emerging technology is under growing interest and many research projects are under development. Nowadays, various chipless designs that embed significant amount of data can be found in literatures.

The method used to encode data in a chipless tag is very different when compared to traditional tags. In this case, data is encoded by changing the electromagnetic footprint of the tag. When a plane wave impinges on the tag, part of the wave is reflected back having a spectrum that depends on the tag shape and composition. To best describe this emerging technology, it is necessary to address a comparison between the two major identification systems, which are the optical barcode and the classical RFID. Like classical RFID, chipless RFID also has advantages such as the better read range and the possibility to read the tag in non line-of-sight, even if it is roughly positioned. Moreover, as for classical RFID some smart functionalities such as sensing can be added to a chipless tag [3].

Chipless tag is roughly composed of metallic strips and made of one piece. To realize it, etching processes can be used, and for some designs, printing techniques are also allowed. This potentially leads to a unit cost comparable to that of the optical barcode.

Unlike classical RFID where anti-collision management is a part of the protocol, in chipless tag anti-collision cannot be implemented. However some techniques based on time or spatial separation of tags can be used. An antenna with narrow beam width can be designed for this purpose [4], but the main weaknesses of chipless technology concerns their non-rewritable capability and their data capacity limited to a few tens of bits. This last characteristic could be a limiting factor for many applications, and this is why work has to be done to increase the data capacity of chipless tags.

The first RFID chipless tag system was introduced by Hartmann *et al.* [5], and uses transient domain for data encoding. The incident pulse from the reader is received by the tag antenna and guided into a SAW (Surface Acoustic Wave) substrate. Several reflectors are set along the substrate to create reflected pulses at specific times. Depending on the reflected pulse position, an identifier can be extracted as in PPM (Pulse Position Modulation) modulation scheme. A coding capacity of 256 bits is possible. To reduce the unit costs of this tag, some designs were proposed using classical low-k substrate [6], [7]. But at the present time, only a few bits can be encoded within a very large structure.

The design presented in this paper enters in a second family of chipless tags that uses the frequency spectrum to encode data. In 2005, Jalaly *et al.* [8] presented a tag that encodes 5 bits with 5 microstrip dipole resonators. The data was encoded by controlling the presence/absence of resonance at a known frequency. Using the same coding technique, Preradovic *et al.* has proposed a tag based on multiple spiral resonators [9], [10] and was able to encode 35 bits. This design is efficient in terms of coding capacity but needs a large size (7 cm × 15 cm) since one bit is equal to one resonator. The phase can also be used to encode data and several techniques have been experimented. Mukherjee *et al.* [11] uses a wideband antenna as a reflector connected to a complex load that can produce different phase profiles. For each phase profile an identifier is associated. Balbin *et al.* [12] use multiple patch antennas connected to a stub of variable length and encodes data by varying the phase of each antenna independently. But at the present time, coding capacity is not significant (few bits).

None of the works presented in the literature for chipless tags had a discussion regarding the way to increase the coding efficiency. However this is still a big challenge to embed a large number of data into a tag of size similar to that of a credit card (5 cm × 8 cm). In the proposed design of this paper, we emphasize a way to increase the coding efficiency in order to reach a high number of combinations with few resonators. To do so, for the first time, we exploit a hybrid coding technique to generate an identifier combining phase deviation technique [13] and frequency shift encoding [14].

In the Section II, a study of several scatterers, also called ECP (Elementary Coding Particle), is presented. Then a tag design made of multiple ECP is presented. In Section III, the new hybrid coding technique is explained. For the sake of comparison, the concept of constellation diagram for frequency domain is introduced. The Section IV presents the measurement and the obtained results that validate the design. Then a discussion on the performance of the chipless tag in terms of coding capacity and ways to improve it concludes this paragraph.

II. Design of the Tag

A. Detail of the Structure

The specific design presented in this section is based on the association of multiple uncoupled resonating elements or ECP. To get the smallest size, each resonating element plays the role of an antenna and a resonator. The most critical parameter is the quality factor of resonators because it defines the resolution frequency of the reading system and the amount of data that can be encoded in a given frequency range.

In Fig. 1, various ECP based metallic strips have been studied to choose a basic shape presenting a good selectivity and a reduced size. Table I presents the key parameters for each ECP, such as the 3 dB bandwidth and the RCS (Radar Cross Section) magnitude. Simulation results are obtained by using CST Microwave Studio with plane wave excitation.

One can notice that a simple shorted dipole presents a good level of response but a large bandwidth, while a SRR (Split Ring Resonator), circular or rectangular, is better in terms of selectivity and gives a response level close to -25 dBsm. Finally a simple “C”-like structure gives the best selectivity with a reduced size and an RCS level at resonance close to those of SRR.

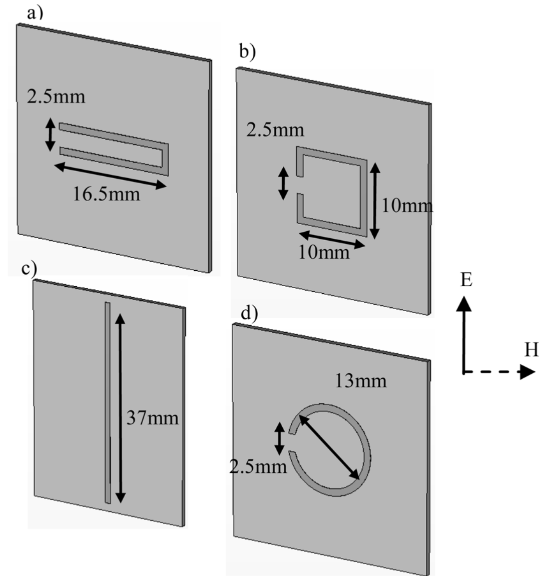

Fig. 1. Scatterers having various shape without ground plane: (a) “C”-like structure, (b) rectangular SRR, (c) shorted dipole, (d) circular SRR. The strip width is 1 mm for all the resonators.

TABLE I
Q Factor and Level Response for Various ECP At 3 GHz

Shape	Resonance Freq. (GHz)	3dB Bandwidth (MHz)	Q factor	|RCS| at resonance (dBsm)
-‘C’-Like	**2.92**	**44**	**65**	**-29.84**
Rect. SRR	2.98	96	30	-25.63
Shorted dipole	2.91	525	5.53	-21
Circ. SRR	2.91	88	33	-26.16

The design presented in Fig. 2 is based on multiple ECP having a “C”-like structure. The substrate used is FR-4 with a permittivity of 4.6, a loss tangent of 0.025 and a thickness of 0.8 mm. The number of resonators for each tag configuration is five, and the size of this structure is nearly 2 cm × 4 cm. For tag 6 and 7, only the slot length is modified keeping the gap constant (0.5 mm). For tag 3, 4 and 5, the gap value is modified between 0.5 and 3.5 mm. This basic ECP is depicted in Fig. 3. This resonator gives a specific electromagnetic footprint when it is impinged by an incident wave. Indeed, in vertical polarization only (see electrical field vector E in Fig. 3) a highly resonant mode can be observed at a specific frequency, which is linked to the physical size of the resonator. Regarding the horizontal polarization, a broadband response is observed so it cannot be used for identification. This structure has intrinsically a resonant mode in its spectrum presenting a peak and an anti-resonant mode giving a dip (see Fig. 4). At the frequency of the peak, the radiation pattern of the C-like resonator is quite isotropic while at the frequency of the dip it has a hole in the direction normal to the resonator surface. The angle of the incident wave (θ in Fig. 3) that impinges the tag is also a critical parameter, since it affects mainly the height of the dip. Thus, to get a significant response,

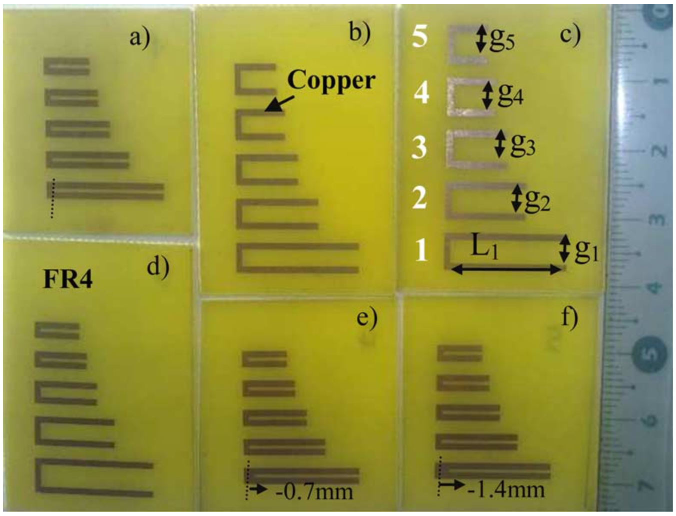

Fig. 2. View of chipless tags (a) tag 1, (b) tag 2, (c) tag 3, (d) tag 5, (e) tag 6, (f) tag 7. Dimensions are given in Table II.

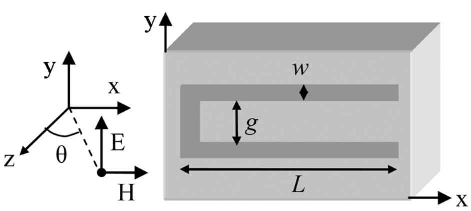

Fig. 3. Basic resonating element based on a metallic strip like-"C" structure.

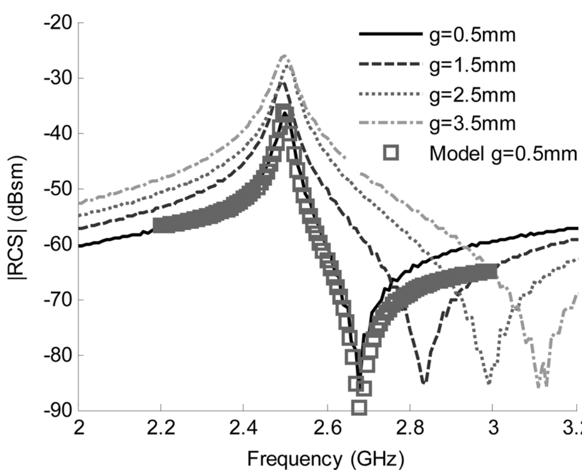

Fig. 4. Simulated and modeled RCS amplitude of a "C" ECP for different gap values. Model parameters according to (1) are $m_p = 0.004, f_p = 2.5$ GHz, $m_z = 0.0025, f_z = 2.68$ GHz and $G = 0.001$.

it was found in simulation that this angle has to be lower than $\pm 45°$.

The frequency values of the peak and the dip can be controlled nearly independently. This behavior is very important since it allows implementing a hybrid coding using two independent coding parameters. The frequency of the peak is linked to the path length $L+g/2$ while separation between the frequencies of peak and dip is controlled by the ratio g/L. Regarding the phase, an interesting behavior can be seen. The resonator behaves as a phase shifter around the resonance (see Fig. 5), and

TABLE II

TAG DIMENSIONS IN mm, AND ASSOCIATED TARGETED CODES

	Tag 1	Tag 2	Tag 3	Tag 4	Tag 5	Tag 6	Tag 7	Tag 8
g1	0.5	1.5	2.5	3.5	3.5	0.5	0.5	0.5
g2	0.5	1.5	2.5	3.5	2.5	0.5	0.5	0.5
g3	0.5	1.5	2.5	3.5	1.5	0.5	0.5	0.5
g4	0.5	1.5	2.5	3.5	0.5	0.5	0.5	0.5
g5	0.5	1.5	2.5	3.5	0.5	0.5	0.5	0.5
L1	18.4	18.9	19.1	19.1	19.1	17.7	17	18.4
L2	12.7	12.7	12.5	12.1	12.5	12.7	12.7	11.7
L3	9.7	9.4	9.2	8.9	9.4	9.7	9.7	9.7
L4	7.8	7.4	7.1	6.7	7.8	7.8	7.8	7.2
L5	6.4	6.1	5.7	5.4	6.4	6.4	6.4	6.4
Code P1	00000	11111	22222	33333	32100	00000	00000	00000
Code P2	00000	00000	00000	00000	00000	10000	20000	30400

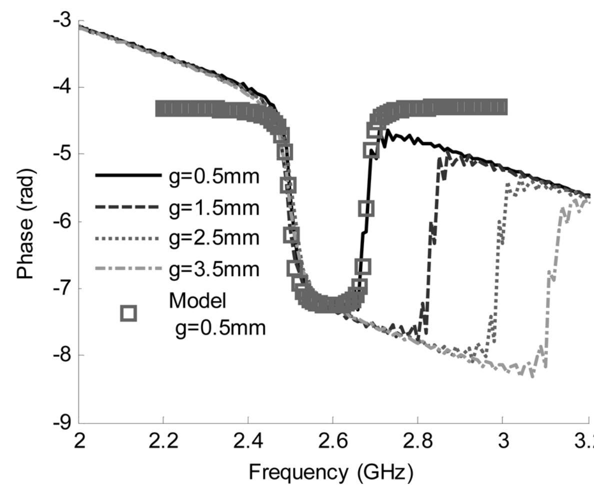

Fig. 5. Simulated and modeled RCS phase of a "C" ECP for different gap values. Model parameters according to (1) are $m_p = 0.004, f_p = 2.5$ GHz, $m_z = 0.0025, f_z = 2.68$ GHz and $G = 0.001$.

its bandwidth is equal to the difference between both the peak and the dip frequencies. To confirm these assumptions, Figs. 6 and 7 respectively show the frequency of the peak as a function of $L+g/2$ and the phase deviation as a function of g/L. Theses values are extracted from the simulations results, varying the length L between 5 and 20 mm and the gap g between 0.5 and 3.5 mm.

B. Model of the Resonator

The amplitude and the phase variations for a "C"-like resonator as a function of the gap g are shown in Figs. 4 and 5 respectively. Even if the loss tangent of FR-4 is relatively high, one can observe some sharp peaks, and significant phase changes. Indeed, the way of radiation is different that for a patch resonator [8], [12]. In this case, there is no cavity mode between the strip and the ground plane. The field lines are not concentrated into the substrate. Consequently, the quality factor of the resonance is no so affected as for patch resonator. In this example, for a given gap g, the slot length L is adjusted in order to have a peak at 2.5 GHz. As explained previously, the dip depends on ratio g/L and as a general rule; a lower ratio reduces the separation between the frequencies of dip and peak. Thanks to simulation results of Fig. 4, it can be determined that a larger

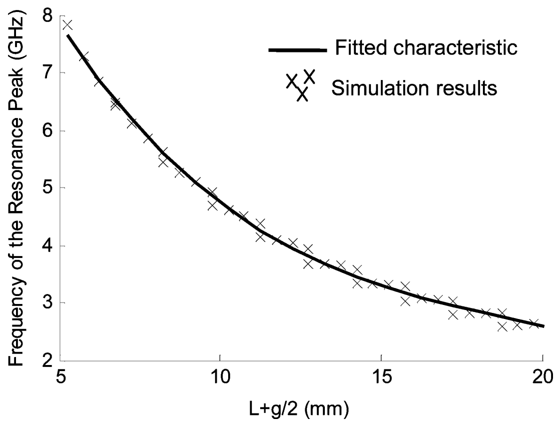

Fig. 6. Relation between the frequency of the resonance peak and length parameters $L + g/2$. A fitted characteristic is obtained based on 44 simulations with various length L and gap g.

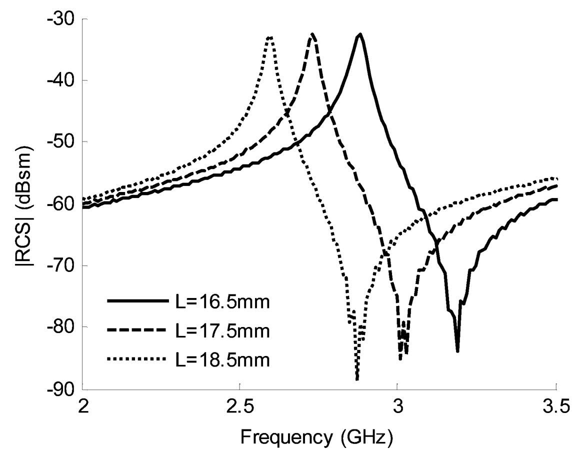

Fig. 8. Simulated RCS amplitude of a C shape for different length L values and a constant gap value $g = 1.5$ mm.

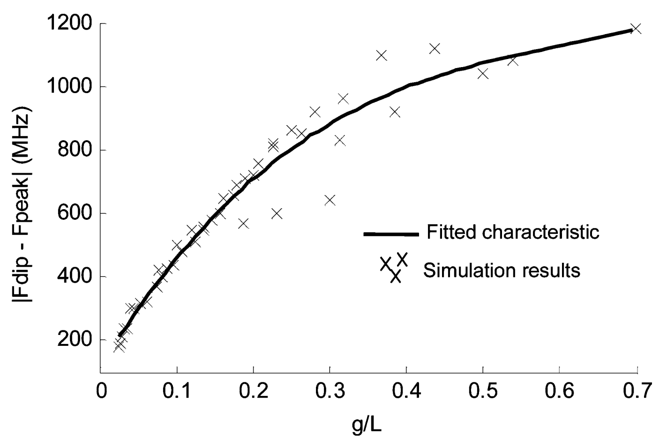

Fig. 7. Separation between the frequencies of peak and dip as a function of length ratio g/L. A fitted characteristic is obtained based on 44 simulations with various length L and gap g.

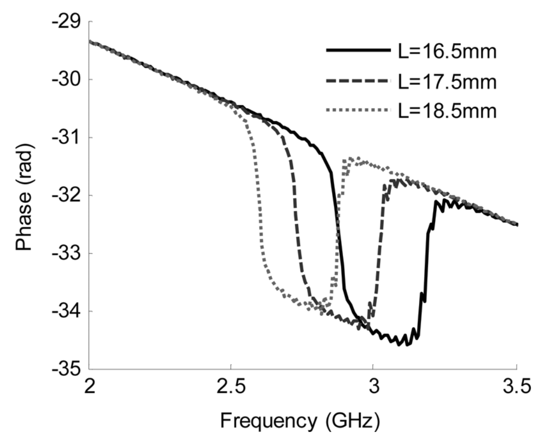

Fig. 9. Simulated RCS phase of a C shape for different length L values. and a constant gap value $g = 1.5$ mm.

gap g means a lower capacitive effect between the two arms of the 'C' ECP. Therefore the attenuation dip is shifted towards high frequency. As a result, the phase shift of value close to $-\pi$ has a larger bandwidth when the gap g increases.

The general response of Fig. 4 can be modeled by an analytical form given by (1). The later can be used to fit the response of any "C"-like resonator

$$\mathsf{T}(\omega) = \mathsf{G}\left[\frac{1 + \frac{2m_z j\omega}{\omega_z} + \left[\frac{j\omega}{\omega_z}\right]^2}{1 + \frac{2m_p j\omega}{\omega_p} + \left[\frac{j\omega}{\omega_p}\right]^2}\right]. \quad (1)$$

In this equation, presence of the peak is linked to a pole of second order having angular frequency ω_p and damping factor m_p while the dip is due to a zero having damping factor m_z and angular frequency ω_z. The gain G characterizes the level of the backscattered signal by the structure.

In Figs. 4 and 5, this model is applied to fit the simulation results of a structure having a gap $g = 0.5$ mm. The model provides good accuracy around the resonance under consideration. To have a closed-form formula valid in the whole bandwidth, it is necessary to add some effects due to quasi-optical reflecting behavior of the tag for higher frequency. This leads to an increase in the amplitude for higher frequencies.

Now, considering the slot length L, changing its value will shift the resonance frequency of the peak, but the phase deviation keeps the same bandwidth as shown in Figs. 8 and 9. Such an interesting behavior will be used in order to implement the hybrid coding technique that uses these two quasi independent variables: the gap g and the length L.

III. CODING TECHNIQUES

As previously discussed, chipless tag did not work with any modulation scheme, so that the coding capacity depends on the number of resonators used and the method of coding. As a result, the capacity of coding is strongly linked to the physical size of the tag for time domain and frequency domain coding approaches.

The idea is to perform the coding efficiency for a given resonator to get a large data capacity. Indeed, if one resonator can encode many bits instead of just one, as for most of previous design that use absence/presence coding technique [8], [9] [see

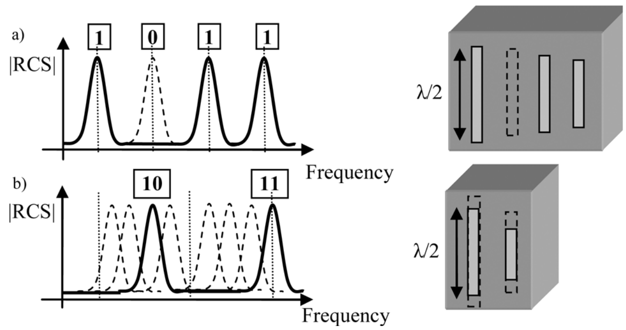

Fig. 10. (a) Absence/presence coding technique introduced by Jalaly [8]. (b) Frequency shift coding technique [13].

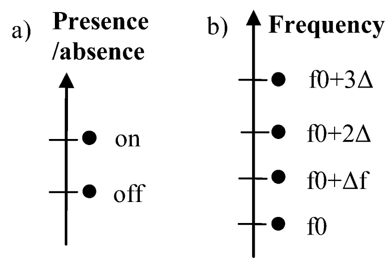

Fig. 11. Constellation diagram (a) for absence/presence coding technique [7], (b) for frequency shift coding technique [11].

Fig. 10(a)], it will lead to a real and a huge improvement in coding capacity per surface.

A first improvement was made by increasing the number of states per resonator, and a previous work using a frequency position coding technique demonstrated the possibility to encode more than 3 bits for each resonator [13]. The used technique is shown in Fig. 10(b).

As for classical modulation scheme in the time domain, a graphic representation of the number of combination that can be encoded for a given symbol i.e., a constellation diagram can be plotted (see Fig. 11) in the frequency domain. Now, if we change more than one parameter for a given resonator, such as the frequency position, the magnitude, the phase or the quality factor, a much higher number of combinations should be possible. The present tag was designed to encode two independent parameters, the phase deviation and the frequency position in a given frequency channel. The way used to encode data due to the phase of a specific mode is illustrated in Fig. 12. As explained previously, by changing the gap g, the phase shape is modified. Similarly, changing the length L shifts the frequency of both the peak and the dip. When the peak and the dip are very close, the phase deviation is narrow and inversely the phase deviation is broad when peak and dip are much more separated.

In the example of Fig. 12, a data value “00” means a narrow phase deviation and a resonance peak at 2.5 GHz while “01” stands for a wide phase deviation and keeping the resonance peak at 2.5 GHz. The Code “10” and “11” are respectively due to a narrow and a wide phase deviation when the peak frequency is equal to 3 GHz. In this simple example using only one resonator, two different values for two different geometric parameters, it is possible to encode 2 bits.

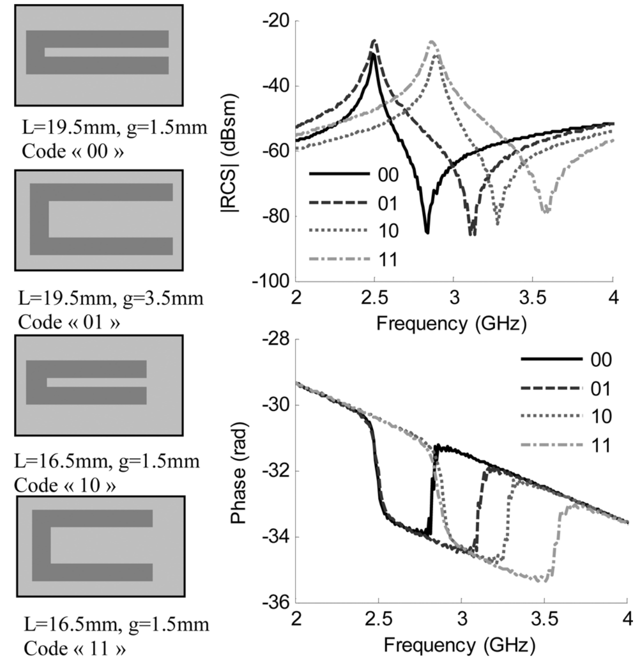

Fig. 12. Coding principle using both phase and frequency shift encoding.

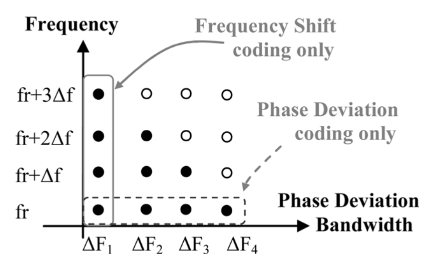

Fig. 13. 2D Constellation diagram for hybrid technique combining phase deviation to frequency shift encoding.

To increase the capacity of coding of the tag, it can be defined more than two values for the frequency of the peak and the phase deviation. As an example with 4 values for each parameter, it can be encoded 4 bits for a single resonator.

To have an idea about the efficiency of the coding introduced here, a 2D frequency constellation diagram is shown in Fig. 13. In this diagram, the sub areas represent the previous combinations used with coding technique based on only one parameter change as for frequency shift coding [14] and phase deviation coding [13]. With this new hybrid coding, a large number of combinations is possible. In Fig. 13, the unfilled circles show the physically impossible states due to resonance overlapping between two adjacent frequency channels.

IV. Measurement Results

A. Measurement Set-Up

Measurement was done in the frequency domain with a Vector Network Analyser HP 8720D having two ports connected to two horn antennas as shown in Fig. 14.

Horn antennas have a gain of 12 dBi in the frequency band of 1 GHz to 18 GHz. Power delivered by VNA is 0 dBm in the

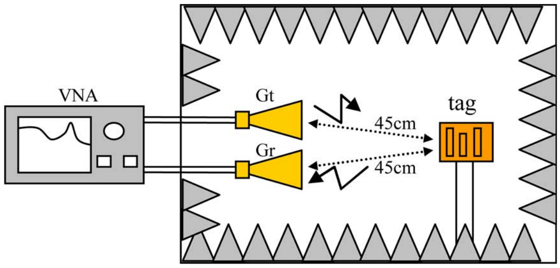

Fig. 14. Measurement set-up using a VNA HP8720D in bi-static configuration. Antennas and tag are put inside an anechoic chamber.

frequency band from 2 GHz to 8 GHz. The tag is placed at a distance of 45 cm from both antennas. Using this configuration, the complex S_{21} parameter is measured. Since the received response on port 2 is very weak, a reference measurement with no tag has to be done. This reference allows removing all static noise due to the environment. Then a measurement with a metallic rectangular plate is done to take into account the effects from antennas. All further measurements with chipless tag are subtracted by isolation measurement and divided by the metallic rectangular plate measurement [15]. This technique allows receiving tag response even in a real environment outside the anechoic chamber. Moreover, because the RCS analytical formula for a metallic rectangular plate is known, it is possible to get an accurate value of the tag RCS using (2)

$$\sigma^{\text{tag}} = \left[\frac{S_{21}^{\text{tag}} - S_{21}^{\text{isolation}}}{S_{21}^{\text{ref}} - S_{21}^{\text{isolation}}}\right]^2 \cdot \sigma^{\text{ref}} \quad (2)$$

where σ^{tag} is the complex RCS value of the tag, σ^{ref} is the complex RCS value of the metallic reference plate obtained with analytical formula and S_{21} are the three measured complex values obtained in bi-static configuration.

RCS is an interesting parameter because it allows providing a power budget of the reading system in order to estimate its Read Range using radar equation [16].

B. Results

The tags shown in Fig. 2 have been realized and measured. The frequency window for each resonator is a function of the total bandwidth available and the number of resonators. Each tag encodes data using 5 resonators and a frequency range between 2.5 and 7.5 GHz is used. Thus each resonator has a channel width of 1 GHz starting at 2.5 GHz, 3.5 GHz, 4.5 GHz, 5.5 GHz and 6.5 GHz. Various gap values g and lengths L are used and data are given in Table II. In addition to the dimensions of the tags, the associated targeted codes P1 and P2 for each configuration are given in the last rows of the table. The code P1 is associated to the phase deviation coding only while the code P2 is linked to the frequency shift coding.

To validate the way of coding, tag 2 to 5 have been realized to vary only the gap g parameter keeping the resonance frequency constant while for tag 6 to 8, only their length L is varied keeping a gap value equal to 0.5 mm. The possible gap values are 0.5 mm, 1.5 mm 2.5 mm and 3.5 mm, to create potentially four phase deviation states for each resonator. The gap

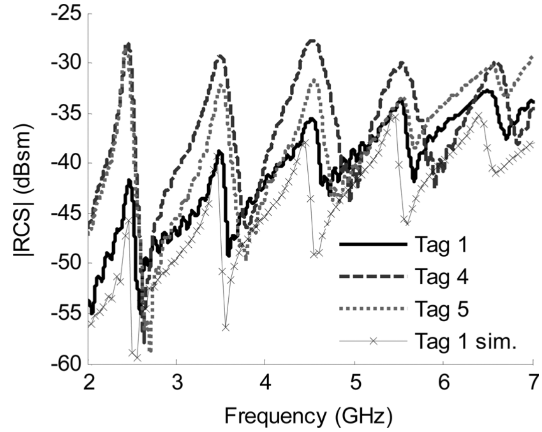

Fig. 15. $|\text{RCS}|$ magnitude measurements for tag 1, 4 and 5.

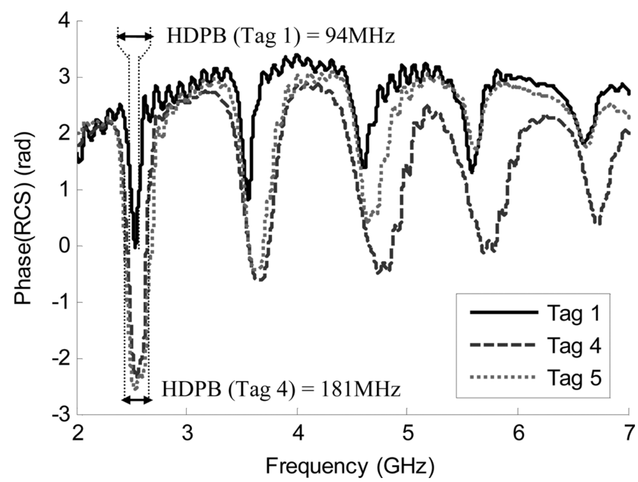

Fig. 16. RCS phase measurements for tag 1, 4 and 5.

increment is constant (1 mm) for sake of simplicity of realization. The tag 1 can be considered as a reference with an identifier equal to "0." Figs. 15 and 16 depict the effect of the gap g. These plots show the frequency response for the tags 1 and 4, having extreme gap values for all the resonators, and for the tag 5 having mixed gap values. In Fig. 15, one can notice that the resonance frequency of each peak is the same irrespective of the gap value. In order to keep constant the resonance frequency while changing the gap g, it is necessary to adjust the length L (it was previously shown in Fig. 6, the correlation between the resonance frequency and $L + g/2$). The RCS level is also modified. A difference ranging from 4 to 15 dB can be observed. To predict measurement results, simulations of the tag have been done. Fig. 15 presents the magnitude of the RCS obtained when the gap g is equal to 0.5 mm. Its value is close to that of the measurement result with a maximal error equal to 4 dB for the peak at 2.5 GHz.

In Fig. 16, measurement results confirm the influence of the gap g on the phase deviation. Concerning the parameter L, Figs. 17 and 18 respectively show the amplitude and the phase of the tag 1, 6 and 7. For these configurations, only the slot length L_1 (see Fig. 2) is modified to produce stepped shifts of 100 MHz for the resonance frequency. In both plots, one can notice that only the first mode is shifted towards higher

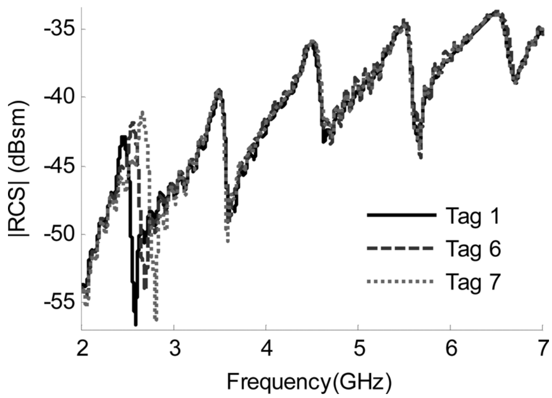

Fig. 17. $|\mathrm{RCS}|$ magnitude measurements for tag 1, 6 and 7.

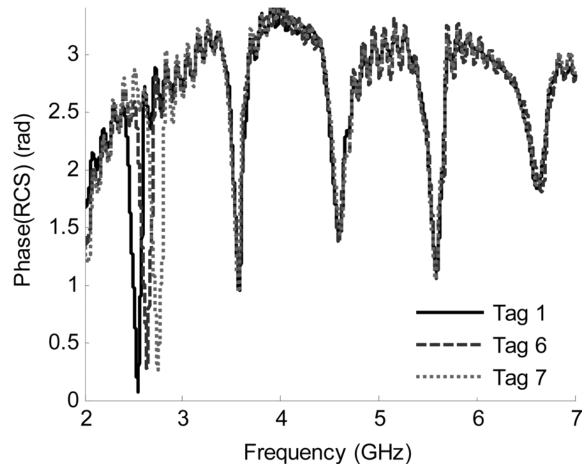

Fig. 18. RCS phase measurements for tag 1, 6 and 7.

frequencies when the length L_1 decreases. The phase deviation bandwidth is kept constant and close to 90 MHz.

A summary of the results for all the tag samples is presented in the Table III. This table was obtained from the phase response. For each mode, the bandwidth corresponds to the frequency for which the phase change (as explained in Section III) is larger than half of its maximum value. This means that observing the phase of tag 4 at 2.5 GHz in Fig. 16, the maximum deviation is 4.5 rad. Thus, the half deviation phase bandwidth (HDPB) is equal to 181 MHz. Tag 1 corresponding to the code "00000" has a narrower bandwidth for each resonance while tag 4 corresponding to the code "33333" has a wider bandwidth. Tag 1 to 4 could be taken as reference for other configurations in order to retrieve the right code depending on the phase deviation for each mode. For tag 5, 6, 7 and 8, color of cells are linked to the closest values obtained for references tags and for a given mode. For example, it can be seen that the first mode of the tag 5 has a bandwidth of 239.5 MHz higher than 181 MHz of the tag 4, coding a "3." And both higher modes have bandwidth very close to the code "0" with a maximum error of 17.5 MHz. It is worth noting that for the reference tag 1 to 5 there is no decoding error even if from tag 4 to tag 5, the frequency variation of the mode 1 is significant (58.5 MHz) while keeping constant g_1. These shifts are due to parameters variations of the nearby resonators. Optimizing the gap increments could be a solution to discriminate all the combinations with a better reliability. In the Table III, one error can be observed for tag 8, since for mode 4, a phase deviation equal to 180.5 MHz is measured coding a "1," even if the gap g is 0.5 mm for this configuration. This unwanted effect seems to be due to the rough slot length reduction necessary to shift the peak frequency from 5.5 GHz to 5.9 GHz. To limit this unwanted effect, a possible way is to slightly change the gap g while changing the length L to keep the ratio g/L constant.

TABLE III
HALF DEVIATION PHASE BANDWIDTH IN MHz AS A FUNCTION OF TAG CONFIGURATION

Tag name	Bandwidth for each resonant mode (MHz)					Code P1
	Mode 1	Mode 2	Mode 3	Mode 4	Mode 5	
Tag 1	93.5	104.5	147	133	135	00000
Tag 2	97.5	152	227	183.5	167.5	11111
Tag 3	145.5	227.5	315	284	209	22222
Tag 4	181	296.5	376.5	357	223	33333
Tag 5	239.5	249	237.5	120	117.5	32100
Tag 6	87	100	131.5	133.5	128	00000
Tag 7	92.5	89	143	127.5	140.5	00000
Tag 8	93	105	133.5	180.5	115.5	00010

TABLE IV
FREQUENCY OF THE RESONANCE PEAK IN MHz AS A FUNCTION OF TAG CONFIGURATION

Tag name	Frequency for each resonant mode (GHz)					Code P2
	Mode 1	Mode 2	Mode 3	Mode 4	Mode 5	
Tag 1	2.45	3.49	4.49	5.5	6.5	00000
Tag 2	2.43	3.47	4.51	5.5	6.54	00000
Tag 3	2.41	3.48	4.55	5.53	6.57	00101
Tag 4	2.42	3.49	4.54	5.52	6.59	00001
Tag 5	2.4	3.49	4.54	5.52	6.53	00000
Tag 6	2.55	3.48	4.5	5.49	6.53	10000
Tag 7	2.66	3.47	4.5	5.49	6.51	20000
Tag 8	2.45	3.78	4.53	5.87	6.51	03040

The frequency values of the resonance peaks for all the configurations are gathered in the Table IV. The tag 1 could be still taken as reference because it defines all starting frequency. A frequency step of 100 MHz is chosen to discriminate two contiguous values so for the first mode the tag 1 with 2.45 GHz gives "0," the tag 6 with 2.55 GHz gives "1" and the tag 7 with 2.66 GHz gives "2." Tag 8 produces the code "03040" since the frequency of the mode 2 is equal to 3.78 GHz, making a difference of 290 MHz with tag 1. For the mode 4, a difference of 370 MHz with respect to the reference gives the value "4." A decoding error can be observed for tags 3 and 4 due to unwanted shifts on modes 3 and 5. These shifts equal to 90 MHz for the larger one, can be limited during the design using a more accurate simulation model. Also, one of the reasons to this effect could be the tolerance of fabrication, roughly ± 50 μm that becomes critical for the highest frequencies. At 6.5 GHz, 50 μm length uncertainties provide a frequency shift of 50 MHz.

C. Discussion

The obtained results confirm the possibility to combine two nearly independent parameters, the phase deviation and the frequency position, to encode data. Measurements in the frequency domain validate this principle of design and confirm the theoretical predictions of coding.
When dealing with a real application, in addition to the design of the tag, it is mandatory to develop the RFID chipless reader. In the literature, it can be found a design of a reading system that uses a YIG oscillator to sweep a CW interrogation signal in the band of interest [17]. However, any reader must be compliant with existing regulations and standards. So, considering the needed frequency band of this chipless tag (5 GHz), it is straightforward to choose the UWB regulation.

The Federal Communications Commission (FCC) defines a power spectral density (PSD) of -41.3 dBm for the band from 3.1 to 10.6 GHz. If sending a CW signal, that means that the signal has to be very week. But the possible way could be to develop an impulse radio based approach. In this case a monocycle pulse of width lower than 100 ps is send by the reader but with a very low duty cycle. The minimum is 1 pulse per μs (i.e., a duty cycle of 0.01%) [18]. If calculating the PSD of this signal, the value is very low even if having a peak amplitude of several volts. However the emitted power during this short time is very high, so the detection of the backscattered response from the tag is possible. Moreover, in case of a noisy environment, to increase the SNR (signal to noise ratio), averaging technique can be used. We have experimented this technique for the detection of chipless tags [14], [19], and a detection range of 50 cm was possible outside anechoic chamber. By using a LNA and increasing the emitting power it is possible to reach 1m range while being compliant with the FCC regulations for UWB communications. On the other hand, for security applications, the reading range is not a key factor (access control) and as it was demonstrated in [20], a chipless tag can be designed to be read into a waveguide. In this case only, the limitation on the emitting power does not matter, since it is confined inside the waveguide. This promising technique could be applied to all the chipless tag designs having no ground plane, since a transmission measurement is done.

For most of the RFID applications, it is needed to put the tag on items of various shapes, thickness and material. In this case, because the structure has no ground plane, its electromagnetic signature is largely influenced by the item's parameters. A large permittivity will largely shift the resonance while a large loss tangent will reduce it. To overcome this practical issue two strategy can be adopted.

The first one consists in designing tags for specific items. In this case the permittivity of the item is taken into account and the parameters of the tag can be corrected to provide the resonance frequencies at chosen locations. For a huge majority of practical applications, this solution could not be used.

The second approach is more effective and promising and can be used for items having a certain permittivity ranges (for example between 1 and 5). It consists in using one or more resonators not to encode information but to probe the effective permittivity of the surrounding environment. In free space, we get a resonance frequency that can be taken as reference (this value is known). The geometry of this resonator will be fixed. Now, if the tag is applied on an object, this resonance frequency will be shifted towards lower frequency. Experimentally we had verified that the relative frequency shift of this probe resonator is linked by a predictive quasi-linear relation to the other resonance frequencies. Consequently, a compensation technique based on the relative frequency shift of the probe can be used and more likely integrated into the reader system.

The design presented in this paper encodes data using two independent parameters, so it can be allocated two independent codes for each resonator. Regarding the phase deviation, the gap can take 4 values from 0.5 mm to 3.5 mm making 4 phase deviations that are clearly visible both in simulation and measurement. As a result, 4 states can be encoded using only this first parameter. Considering the frequency of the peak, since a frequency step of 100 MHz has been chosen and that each mode can vary on a 900 MHz frequency span (i.e., from 2.5 to 3.4 GHz for the first mode and so on) one can consider that 10 states can be encoded. But in reality, the maximum phase deviation bandwidth can reach 400 MHz from the peak, so it is necessary to limit the maximal shift for the peak to 500 MHz from the starting frequency of each mode. As a result, the number of states that can be encoded for this second parameter is 6. Finally the number of combinations that can be encoded for each resonator using both parameters is equal to $4 \times 6 = 24$. For the 5 resonators that are used the total number of combinations is equal to $24^5 = 7\,962\,624$, i.e., 22.9 bits within a tag of size 2 cm $\times$ 4 cm.

This corresponds to a density of coding per surface (DPS) of 2.86 bits/cm^2. To compare, previous design from I. Jalaly [7] reaches 0.81 bits/cm^2.

V. Conclusion

The design presented in this work demonstrated for the first time the possibility to use more than one physical dimension in order to control two coding parameters independently. This was possible due to the "C"-like resonator used as Elementary Coding Particle, presenting uncoupled resonance and anti-resonance modes. By combining the phase deviation encoding to the frequency shift encoding, to get a hybrid coding technique, a real improvement is made in terms of coding efficiency. Indeed, instead of having only 10 bits in a previous work [11] where only the phase deviation was used, the coding capacity reach now 22.9 bits within a structure having a reduced size of 2 cm $\times$ 4 cm.

Only one conductive layer has been used for tag fabrication since there is no ground plane. This makes it possible to reach a very low unit cost if using for example printing techniques.

Even if the "C"-like structure of the elementary resonator is very basic, modifying only L and g dimensions make possible a hybrid coding technique and that was confirmed by measurements done in the frequency domain.

In the future work, a chipless tag reading system will be designed working in the operating frequency between 3.1 and 10.6 GHz. A promising way seems to develop an impulse radio based reader to fit the emitting power mask defined by FCC and ECC for UWB communications.

ACKNOWLEDGMENT

The authors are grateful to Grenoble Institute of Technology for supporting this project via the BQR program. They also thank R. Nair for her help on part of this work.

REFERENCES

[1] K. Finkenzeller, *RFID Handbook: Radio-Frequency Identification Fundamentals and Applications*. Hoboken, NJ: Wiley, 2004.

[2] IDTechEx, Printed and Chipless RFID Forecasts, Technologies & Players 2009–2019 [Online]. Available: www.IdtechEx.com

[3] S. Shrestha, M. Balachandran, M. Agarwal, V. V. Phoha, and K. Varahramyan, "A chipless RFID sensor system for cyber centric monitoring applications," *IEEE Trans. Microw. Theory Tech.*, vol. 57, no. 5, pp. 1411–1419, May 2009, pp 1303–1309.

[4] C. Hartmann, P. Hartmann, P. Brown, J. Bellamy, L. Claiborne, and W. Bonner, "Anti-collision methods for global SAW RFID tag systems," in *Proc. IEEE Ultrasonics Symp.*, Montréal, Canada, Aug. 2004, pp. 805–808.

[5] C. S. Hartmann, "A global SAW ID tag with large data capacity," in *Proc. IEEE Ultrasonics Symp.*, Munich, Germany, Oct. 2002, pp. 65–69.

[6] L. Zheng, S. Rodriguez, L. Zhang, B. Shao, and L.-R. Zheng, "Design and implementation of a fully reconfigurable chipless RFID tag using Inkjet printing technology," in *Proc. IEEE Int. Symp. on Circuits And Systems*, Seattle, WA, May 2008, pp. 1524–1527.

[7] C. Mandel, M. Schüßler, M. Maasch, and R. Jakoby, "A novel passive phase modulator based on LH delay lines for chipless microwave RFID applications," presented at the IEEE MTT-S Int. Microwave Workshop on Wireless Sensing, Local Positioning, and RFID, Cavtat, Croatia, Sep. 24–29, 2009.

[8] I. Jalaly and D. Robertson, "RF barcodes using multiple frequency bands," in *IEEE MTT-S Microwave Symp. Dig.*, Long Beach, CA, Jun. 2005, pp. 139–141.

[9] S. Preradovic, S. Roy, and N. C. Karmakar, "Fully printable multi-bit chipless RFID transponder on flexible laminate," in *Proc. Asia-Pacific Micro. Conf.*, Singapore, Dec. 2009, pp. 2371–2374.

[10] S. Preradovic, I. Balbin, N. C. Karmakar, and G. F. Swiegers, "Multiresonator-based chipless RFID system for low-cost item tracking," *IEEE Trans. Microw. Theory Tech.*, vol. 57, no. 5, pp. 1411–1419, May 2009.

[11] S. Mukherjee, "Chipless radio frequency identification by remote measurement of complex impedance," in *Proc. 37th Euro. Microwave Week*, Munich, Germany, Oct. 2007, pp. 1007–1010.

[12] I. Balbin and N. C. Karmakar, "Phase-encoded chipless RFID transponder for large-scale low-cost applications," *IEEE Microw. Wireless Compon. Lett.*, vol. 19, no. 8, pp. 509–511, Aug. 2009.

[13] A. Vena, E. Perret, and S. Tedjini, "RFID chipless tag based on multiple phase shifters," presented at the IEEE MTT-S Int. Microwave Symp. Dig., Baltimore, MD, Jun. 5–10, 2011.

[14] A. Vena, E. Perret, and S. Tedjini, "Novel compact RFID chipless tag," presented at the Proc. Progress in Electromagnetic Research Symp., Marrakesh, Morocco, Mar. 20–23, 2011.

[15] W. Wiesbeck and D. Kähny, "Single reference, three target calibration and error correction for monostatic, polarimetric free space measurements," *Proc. IEEE*, vol. 79, no. 10, pp. 1551–1558, Oct. 1991.

[16] C. A. Balanis, Antenna Theory, Analysis and Design. New York, Wiley-Interscience3rd ed. , 2005.

[17] S. Preradovic and N. C. Karmakar, "Multiresonator based chipless RFID tag and dedicated RFID reader," in *IEEE MTT-S Int. Microwave Symp. Dig.*, Anaheim, CA, May 2010, pp. 1520–1523.

[18] S. Härmä, V. P. Plessky, X. Li, and P. Hartogh, "Feasibility of ultra-wideband SAW RFID tags meeting FCC rules," *IEEE Trans. Ultrason., Ferroelect. Freq. Control*, vol. 56, no. 4, Apr. 2009.

[19] A. Vena, T. Singh, E. Perret, and S. Tedjini, "Metallic letter identification based on radar approach," presented at the URSI GASS, Istanbul, Turkey, Aug. 13–20, 2011.

[20] H.-S. Jang, W.-G. Lim, K.-S. Oh, S.-M. Moon, and J.-W. Yu, "Design of low-cost chipless system using printable chipless tag with electromagnetic code," *IEEE Microw. Wireless Compon. Lett.*, vol. 20, no. 11, pp. 640–642, Nov. 2010.

Arnaud Vena received the Eng. Dipl. degree in electrical engineering from the Institut National Polytechnique de Grenoble (Grenoble-INP), Grenoble, France, in 2005, where he is currently working toward the Ph.D. degree.

From 2005 to 2009, he worked as an R&D Engineer at ACS Solution France SAS. He was in charge of development of RFID contactless card readers and contributed to evolution of the ISO/IEC 14443 regulation. In October 2009, he started his research with the Grenoble Institute of Technology, mainly focused on design of chipless RFID systems.

Etienne Perret (M'05) was born in Albertville, Savoie, France, on October 30, 1979. He received the Eng. Dipl. degree in electrical engineering from the Ecole Nationale Supérieure d'Electronique, d'Electrotechnique, d'Informatique, d'Hydraulique, et des Télécommunications, Toulouse, France, in 2002, and the M.Sc. and Ph.D. degrees from the Toulouse Institute of Technology, France, in 2002 and 2005, respectively, all in electrical engineering.

From 2005 to 2006, he held a postdoctoral position at the Institute of Fundamental Electronics (IEF), Orsay, France. His research activities cover the electromagnetic modeling of passive devices for millimeter and submillimeter-wave applications. His current research interests are in the field of wireless communications, especially radio frequency identification (RFID) with the design and development of antennas for RFID tags. Since September 2006, he is an Assistant Professor of electronics at the Grenoble Institute of Technology. He has authored and coauthored more than 50 technical conferences, letters and journal papers, and one book chapter.

Dr. Perret is a Technical Program Committee member of IEEE-RFID. He was keynote speaker and the Chairman of the 11th Mediterranean Microwave Symposium MMS'2011. He also served as the Co-Chair of the 29th PIERS 2011 in Marrakesh, Morocco.

Smail Tedjini (SM'92) received the Doctor in physics degree from Grenoble University, Grenoble, France, in 1985.

He was an Assistant Professor from 1981 to 1986, and Senior Researcher for the CNRS from 1986 to 1993. He became University Professor in 1993 and since 1996 he is a Professor at the ESISAR Department, Institut National Polytechnique de Grenoble (Grenoble-INP), Grenoble, France. His specialization topics concern electromagnetism, RF, wireless and optoelectronics. He serves as coordinator and staff member in numerous academic programs both for education and research. In 2006 to 2007, he served as the Director of ESISAR, Embedded Systems Department, Grenoble-INP. He is involved in academic research supervision since 1982. He is the Founder and past Director of the LCIS Lab. Now, he is the ORSYS Group Leader. His main topics in research are applied electromagnetism, modeling of devices and circuits at both RF and optoelectronic domains. Current research concerns wireless systems with specific attention to RFID and nanoRF. He supervised 27 Ph.D. candidates and he has more than 250 publications.

Dr. Tedjini is a member of several TPC and serves as expert/reviewer for national and international scientific committees and conferences including ISO, Piers, IEEE, URSI, ISO, ANR, OSEO, FNQRT… He organized several conferences/workshops. He is President and founder of the IEEE-CPMT French Chapter, Vice-President of IEEE Section France and elected as the Vice-Chair of URSI Commission D "Electronics & Photonics" in 2008. He was reelected as Vice-Chair of the IEEE-France section and will serve as the Chair of URSI Commission "D3" for the triennium 2011–2014.

射 频 和 天 线 设 计 培 训 课 程 推 荐

易迪拓培训(www.edatop.com)由数名来自于研发第一线的资深工程师发起成立，致力并专注于微波、射频、天线设计研发人才的培养；我们于 2006 年整合合并微波 EDA 网(www.mweda.com)，现已发展成为国内最大的微波射频和天线设计人才培养基地，成功推出多套微波射频以及天线设计经典培训课程和 ADS、HFSS 等专业软件使用培训课程，广受客户好评；并先后与人民邮电出版社、电子工业出版社合作出版了多本专业图书，帮助数万名工程师提升了专业技术能力。客户遍布中兴通讯、研通高频、埃威航电、国人通信等多家国内知名公司，以及台湾工业技术研究院、永业科技、全一电子等多家台湾地区企业。

易迪拓培训课程列表：http://www.edatop.com/peixun/rfe/129.html

射频工程师养成培训课程套装

该套装精选了射频专业基础培训课程、射频仿真设计培训课程和射频电路测量培训课程三个类别共 30 门视频培训课程和 3 本图书教材；旨在引领学员全面学习一个射频工程师需要熟悉、理解和掌握的专业知识和研发设计能力。通过套装的学习，能够让学员完全达到和胜任一个合格的射频工程师的要求…

课程网址：http://www.edatop.com/peixun/rfe/110.html

ADS 学习培训课程套装

该套装是迄今国内最全面、最权威的 ADS 培训教程，共包含 10 门 ADS 学习培训课程。课程是由具有多年 ADS 使用经验的微波射频与通信系统设计领域资深专家讲解，并多结合设计实例，由浅入深、详细而又全面地讲解了 ADS 在微波射频电路设计、通信系统设计和电磁仿真设计方面的内容。能让您在最短的时间内学会使用 ADS，迅速提升个人技术能力，把 ADS 真正应用到实际研发工作中去，成为 ADS 设计专家...

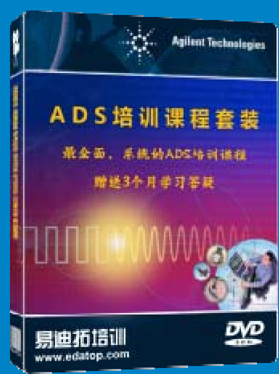

课程网址： http://www.edatop.com/peixun/ads/13.html

HFSS 学习培训课程套装

该套课程套装包含了本站全部 HFSS 培训课程，是迄今国内最全面、最专业的 HFSS 培训教程套装，可以帮助您从零开始，全面深入学习 HFSS 的各项功能和在多个方面的工程应用。购买套装，更可超值赠送 3 个月免费学习答疑，随时解答您学习过程中遇到的棘手问题，让您的 HFSS 学习更加轻松顺畅…

课程网址：http://www.edatop.com/peixun/hfss/11.html

CST 学习培训课程套装

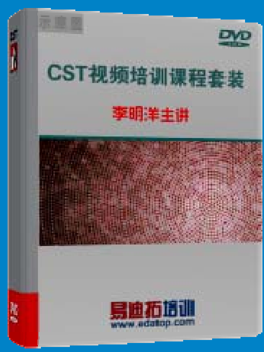

该培训套装由易迪拓培训联合微波 EDA 网共同推出，是最全面、系统、专业的 CST 微波工作室培训课程套装，所有课程都由经验丰富的专家授课，视频教学，可以帮助您从零开始，全面系统地学习 CST 微波工作的各项功能及其在微波射频、天线设计等领域的设计应用。且购买该套装，还可超值赠送 3 个月免费学习答疑…

课程网址：http://www.edatop.com/peixun/cst/24.html

HFSS 天线设计培训课程套装

套装包含 6 门视频课程和 1 本图书，课程从基础讲起，内容由浅入深，理论介绍和实际操作讲解相结合，全面系统的讲解了 HFSS 天线设计的全过程。是国内最全面、最专业的 HFSS 天线设计课程，可以帮助您快速学习掌握如何使用 HFSS 设计天线，让天线设计不再难…

课程网址：http://www.edatop.com/peixun/hfss/122.html

13.56MHz NFC/RFID 线圈天线设计培训课程套装

套装包含 4 门视频培训课程，培训将 13.56MHz 线圈天线设计原理和仿真设计实践相结合，全面系统地讲解了 13.56MHz 线圈天线的工作原理、设计方法、设计考量以及使用 HFSS 和 CST 仿真分析线圈天线的具体操作，同时还介绍了 13.56MHz 线圈天线匹配电路的设计和调试。通过该套课程的学习，可以帮助您快速学习掌握 13.56MHz 线圈天线及其匹配电路的原理、设计和调试…

详情浏览：http://www.edatop.com/peixun/antenna/116.html

我们的课程优势：

※ 成立于 2004 年，10 多年丰富的行业经验，

※ 一直致力并专注于微波射频和天线设计工程师的培养，更了解该行业对人才的要求

※ 经验丰富的一线资深工程师讲授，结合实际工程案例，直观、实用、易学

联系我们：

※ 易迪拓培训官网：http://www.edatop.com

※ 微波 EDA 网：http://www.mweda.com

※ 官方淘宝店：http://shop36920890.taobao.com